Anal. Chem. **2006,** *78,* 1052−1060

Integrated Description of Electrode/Electrolyte Interfaces Based on Equivalent Circuits and Its Verification Using Impedance Measurements

Byoung-Yong Chang and Su-Moon Park*

Department of Chemistry and Center for Integrated Molecular Systems, Pohang University of Science and Technology, Pohang, Gyeongbuk 790-784, Korea

An integrated theory describing both faradaic and nonfaradaic currents obtained upon potential step at an electrified electrode/electrolyte interface has been developed based on equivalent circuits that had been used to explain electrochemical reactions and experimentally verified. The faradaic current is shown to consist of the mass transport-dependent and -independent parts, which is in general agreement with the expression previously derived from the diffusion equations. The decay of the capacitive current is determined by the time constant represented by the product of the resistance obtained from the parallel connection of the solution and polarization resistances and the double layer capacitance; this is not consistent with the current understanding of the capacitive current decay, which takes into account the double layer capacitance and the solution resistance only. Many insights into the electron-transfer reactions are discussed based on the interpretation of impedance representation of the system, which would not have been possible without the present theory.

An electrode/electrolyte interface cannot be fully described without information on its electrical characteristics, which can only be obtained from the electrochemical impedance spectroscopic (EIS) measurements.[1−4] A full description of the interface has been hampered by the inability of the traditional techniques to make the impedance measurements without perturbing electrochemical systems during the experiments.[5] This is because the state-of-the-art of impedance measurements utilize a frequency response analyzer (FRA), which generates a series of ac waves of various frequencies, overlay with a dc bias potential, applies the signals to an electrochemical system of interest, and makes resulting ac current measurements at each designated frequency.[3,4] The impedances are then calculated from the excitation function, i.e., ac voltage waves, and its response function, i.e., ac currents, obtained from the system of interest. This approach, however, takes a long time to scan the whole range of frequencies, which prompted many investigators to propose faster measurement methods.[6−12] In addition to the time taken for the measurements, its validity has been questioned by many investigators as the measurement requires the system to be established as stationary for reliable results; the need for impedance measurements of nonstationary electrochemical systems has been discussed extensively in the literature.[5]

Of the techniques developed for faster EIS measurements during the past few decades, the one using a concept similar to that used in, for example, nuclear magnetic resonance spectroscopic experiments[12] offers many advantages over the traditional methods. In this technique,[4,12] a small voltage step is applied to an electrochemical system and the first derivative of the current obtained thereof is Fourier transformed into the frequency domain before the impedance calculation is made. Thus the idea is based on the fact that a Dirac δ function, which is the derivative form of the potential step and is also the sum of ac voltage signals of all frequencies with the identical amplitude and phase, is applied to an electrochemical system, and its current response, which would also be the sum of all the ac current waves, is then transformed into the frequency domain by Fourier transform. One problem with this approach, however, is that the δ function cannot be

* To whom correspondence should be addressed. E-mail: smpark@postech.edu. Phone: +82-54-279-2102. Fax: +82-54-279-3399.

(1) Bard, A. J.; Faulkner, L. R. *Electrochemical Methods*; John Wiley and Sons: New York, 2001; Chapter 10.
(2) Schmickler, W. *Interfacial Electrochemistry*; Oxford University Press: Oxford, U.K., 1996.
(3) Macdonald, J. R. *Impedance Spectroscopy*; Wiley/Interscience: New York, 1987.
(4) Park, S.-M.; Yoo, J.-S. *Anal. Chem.* **2003**, *75*, 455A.
(5) (a) Sluyters-Rehbach, M.; Sluyters, J. H. *J. Electroanal. Chem.* **1979**, *102*, 415. (b) Popkirov, G. S.; Schneider, R. N. *Electrochim. Acta* **1993**, *38*, 861. (c) Stoynov, Z. B.; Savova-Stoynov, B. S. *J. Electroanal. Chem.* **1985**, *183*, 133. (d) Savova-Stoynov, B.; Stoynov, Z. B. *Electrochim. Acta* **1992**, *37*, 2353. (e) Stoynov, Z. *Electrochim. Acta* **1992**, *37*, 2357. (f) Stoynov, Z. *Electrochim. Acta* **1993**, *38*, 1919.
(6) (a) Creason S. C.; Smith, D. E. *J. Electroanal. Chem.* **1972**, *36*, 1. (b) Creason S. C.; Smith, D. E. *Anal. Chem.* **1973**, *47*, 2401. (c) Smith, D. E. *Anal. Chem.* **1976**, *48*, 221A, 517A. (d) Schwall, R. J.; Bond, A. M.; Loyd, R. J.; Larsen, J. G.; Smith, D. E. *Anal. Chem.* **1977**, *49*, 1797. (e) Schwall, R. J.; Bond, A. M.; Smith, D. E. *Anal. Chem.* **1977**, 49, 1805. (f) O'Halloran, R. J.; Schaar, J. E.; Smith, D. E. *Anal. Chem.* **1978**, *50*, 1073. (g) Crzeszczuk M.; Smith, D. E. *J. Electroanal. Chem.* **1983**, *157*, 205.
(7) (a) Bond, A. M. *J. Electroanal. Chem.* **1974**, *50*, 285. (b) Ühlken, J.; Waser, R.; Wiese, H. *Ber. Bunsen-Ges. Phys. Chem.* **1988**, *92*, 730. (c) Házi, J.; Elton, D. M.; Czerwinski, W. A.; Schiewe, J.; Vincente-Beckett, V. A.; Bond, A. M. *J. Electroanal. Chem.* **1997**, *437*, 1.
(8) (a) Popkirov, G. S.; Schindler, *Rev. Sci. Instrum.* **1992**, *63*, 5366. (b) Popkirov, G. S. *Electrochim. Acta.* **1996**, *41*, 1023. (c) Darowicki, K.; Kawula, J. *Electrochim. Acta* **2004**, *49*, 4824.
(9) Pilla, A. *J. Electrochem. Soc.* **1970**, *117*, 467.
(10) Smyrl, W. *J. Electrochem. Soc.* **1985**, *132*, 1551.
(11) Barsoukov, E.; Ryu, S. H.; Lee, H. *J. Electroanal. Chem.* **2002**, *536*, 109.
(12) (a) Yoo, J.-S.; Park, S.-M. *Anal. Chem.* **2000**, *72*, 2035. (b) Yoo, J.-S.; Song, I.; Lee, J.-H.; Park, S.-M. *Anal. Chem.* **2003**, *75*, 3294.

10.1021/ac051641l CCC: $33.50
Published on Web 12/24/2005

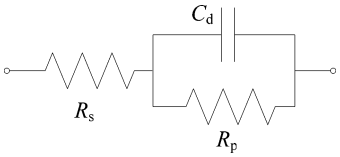

Figure 1. Simple equivalent circuit without a Warburg impedance included.

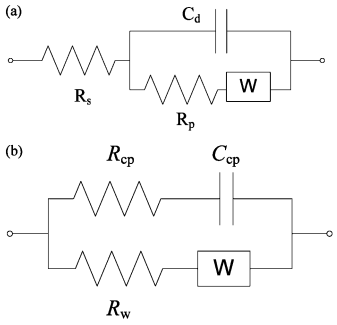

Figure 2. (a) Equivalent circuit with a Warburg impedance included and (b) an equivalent circuit mathematically equivalent to that shown in (a) when R_w, C_{cp}, and R_{cp} are defined by the relations defined in eq 10.

obtained from a known electronic device, and thus, its integrated form, i.e., a step function, is used instead. This procedure requires that the system studied be linear, because a linear system, which gives a response function, $y(t)$, upon application of an excitation function, $x(t)$, would give its integrated or derivative form, $\int y(t)\,dt$ or $y'(t)$, upon application of the integrated or derivative form of the excitation function, $\int x(t)\,dt$ or $x'(t)$.[13] While the electrochemical system is not linear for the current is expressed as an exponential function of the overpotential, the system can be linearized by making the excitation source, i.e., voltage step, small enough.[1]

This method, however, was conducted with only the components displayed in Figure 1 considered for impedance measurements in the original work.[12a] However, an important component, i.e., the Warburg impedance, which results from mass transport taking place during electrochemical reactions, is missing in the equivalent circuit shown in Figure 1. To remove or minimize the effects of the mass transport, the authors ramped the potential to the value at which the bias potential was set and waited there for the system to reach a steady state, and then a small potential step was applied. The current obtained at the bias was then subtracted from that obtained upon potential step. This removed most of the mass transport effects, and the results obtained perfectly fitted the equivalent circuit shown in Figure 1.[12a] Although the problem due to the mass transport was circumvented in this manner, it is true that the equivalent circuit shown in Figure 2a should reflect a real electrochemical cell. Thus, the limitation of this method was pointed out by Jurczakowski and Lasia in their recent publication,[14] in which they showed that reliable data may be obtained only in the frequency range between $1/(N\cdot\Delta t)$ and $1/(2\cdot\Delta t)$, where N is the number of data points acquired during the experiment and Δt is the sampling interval. The sampling period is defined as $N\cdot\Delta t$. The method therefore may show a partial or full picture of the electrochemical interface depending on how fast the mass transport gets into the picture. To show that this was the case, the authors employed the simulated data for a simple ideally polarized electrode using the current expression derived from the diffusion equations and the capacitive current behavior described by the $R_s\cdot C_d$ time constant, where R_s is the solution resistance and C_d is the double layer capacitance.

Two questions arising from our discussion here are, (1) would the Warburg impedance not be seen by the fast impedance measurements and (2) how unreliable would the measurements be if the sampling period is short, e.g., less than 5 ms, as was done in the original work?[12a] In efforts to address these questions and other related aspects, we first derive an expression for the current based solely on the equivalent circuit shown in Figure 2a and verify that the electrochemical behavior can indeed be described by the parameters obtained from electrochemical impedance spectroscopy. This is very important in that the equivalent circuits were first conceived in efforts to explain the impedance behaviors observed for electrochemical systems[15] but are now shown to be a model for describing electrode kinetics in this work. Thus, generalized pictures of electrode/electrolyte interfaces are obtained from the results of EIS measurements, which should represent important progress in the understanding of an electron-transfer process.

EXPERIMENTAL SECTION

Hexaammineruthenium(III) chloride ($Ru(NH_3)_6Cl_3$; Aldrich, 98%), 1,4-benzoquinone (*p*-BQ; Aldrich, 98%), and ferrous sulfate ($FeSO_4\cdot(H_2O)_7$; Acros, Granulated C.P.) were used as electroactive compounds, while potassium chloride (Samchun, 99.0%) and sulfuric acid (Samchun, 99.0%) were used as supporting electrolytes, without further purification. Aqueous solutions were prepared by dissolving an appropriate amount of $Ru(NH_3)_6Cl_3$, *p*-BQ, or $FeSO_4\cdot(H_2O)_7$ and KCl or H_2SO_4 such that the concentrations of the electroactive compound and the supporting electrolyte are 5.0 mM and 0.50 M, respectively. The impedance measurements were made at a gold disk working electrode (diameter 1.8 mm, area 0.025 cm^2) for $Ru(NH_3)_6Cl_3$ and *p*-BQ reduction after it was polished to a mirror finish successively with alumina slurries (Buehler) of 5.0−0.05 μm. For Fe^{2+} oxidation, a boron-doped diamond electrode (BDD; area 0.12 cm^2) was used as a working electrode. The electrochemical cell had three electrodes, the gold disk or BDD working electrode described above, a platinum gauze counter electrode, and a homemade Ag|AgCl (in saturated KCl) reference electrode. The impedance measurements were made with the setup we have assembled with an application of a potential step of 15 mV at a given bias voltage, the details of which are described elsewhere.[12b]

RESULTS AND DISCUSSION

Development of the Theory and Its Examination. When a small potential step is applied to an electrochemical system containing an oxidant and a reductant,

(13) (a) Gabel, R. A.; Roberts, R. A. *Signals and Linear Systems*; Wiley: New York, 1987. (b) Carlson, A. B. *Communication Systems*; McGraw-Hill: Singapore, 1986. (c) Ifeachor, E. C.; Jervis, B. W. *Digital Signal Processing*; Addision-Wesley: New York, 1993.

(14) Jurczakowski, R.; Lasia, A. *Anal. Chem.* **2004**, *76*, 5033.

(15) Randles, E. B. *Discuss. Faraday Soc.* **1947**, *1*, 11.

$$\mathrm{Ox} + e \underset{k_b}{\overset{k_f}{\rightleftharpoons}} \mathrm{Red} \quad (1)$$

the system can be described by the Butler−Volmer equation, which has both the anodic and cathodic terms.[16a] Thus, an expression for current may be obtained for an electrochemical reaction based on the diffusion of the oxidant and reductant as well as a kinetic relation based on the Butler−Volmer equation.[16b] When the potential is in the diffusion-limited region, the current becomes the Cottrell equation, while a more general current expression, I_f, has been shown to be[16b,17]

$$I_f = nFA(k_f C_O^* - k_b C_R^*)\exp(H^2 t)\,\mathrm{erfc}(H\sqrt{t}) \quad (2)$$

with

$$H = \frac{k_f}{\sqrt{D_O}} + \frac{k_b}{\sqrt{D_R}} \quad (3)$$

in which the rates of both forward and backward reactions are factored in. Here n is the number of electrons transferred, F the faraday constant, A the electrode area, C_O^* the bulk concentration of the oxidant, C_R^* the bulk concentration of the reductant, k_f the electron-transfer rate constant for the forward reaction at an overpotential η, k_b the rate constant for the reverse reaction, t the electrolysis time, and D the diffusion coefficient of either the oxidant or the reductant. Thus, the current expression has two parts: the diffusion-independent part, which is originated from the Butler−Volmer kinetics, and the diffusion-dependent part, which results from the solution of diffusion equations.[17] While eq 2 describes the current obtained upon potential step, it does not give any idea of how the current would be expressed in terms of the equivalent circuit.

From strictly the equivalent circuit shown in Figure 1, the current expression has been derived as,[12a]

$$i(t) = U(t)\left[\frac{\Delta V}{R_s} e^{-(R_p+R_s)/(R_p R_s C_d)\cdot t} + \frac{\Delta V}{R_p + R_s}\left(1 - e^{-(R_p+R_s)/(R_p R_s C_d)\cdot t}\right)\right] \quad (4)$$

where ΔV is the step size and $U(t)$ is the unit step function with other symbols defined in Figure 1. This is because the impedance of the circuit has an expression,

$$Z(\omega) = R_s + \frac{R_p}{1 + jR_p C_d \omega} \quad (5)$$

where $\omega = 2\pi f$ with f being the frequency. Thus, we see that eq 4 is made of two components, capacitive (first term) and faradaic (second term) currents, describing the behavior of the cell represented by the equivalent circuit shown in Figure 1. Note that the faradaic component acts in a fashion complimentary to the capacitive component in this expression, where no mass transport is considered.

Now, the impedance expression becomes more complex than eq 5 when the mass transport is taken into account and it is[1]

$$Z(\omega) = R_s + \frac{R_p + \sigma\omega^{-1/2}}{(C_d\sigma\omega^{1/2} + 1)^2 + \omega^2 C_d^2 (R_p + \sigma\omega^{-1/2})^2} - j\frac{\omega C_d (R_p + \sigma\omega^{-1/2})^2 + \sigma\omega^{-1/2}(\sigma\omega^{1/2} C_d + 1)}{(C_d\sigma\omega^{1/2} + 1)^2 + \omega^2 C_d^2 (R_p + \sigma\omega^{-1/2})^2} \quad (6)$$

for the equivalent circuit shown in Figure 2a. Here σ is defined as

$$\sigma = \frac{RT}{\sqrt{2}F^2 A}\left(\frac{1}{\sqrt{D_O} C_O^*} + \frac{1}{\sqrt{D_R} C_R^*}\right) \quad (7)$$

for $n = 1.0$. Equation 6 can now be simplified to

$$Z(s) = R_s + \frac{R_p\sqrt{s} + \sqrt{2}\sigma}{R_p C_d s\sqrt{s} + \sqrt{2}\sigma C_d s + \sqrt{s}} \quad (8)$$

by introducing a relation, $s = j\omega$. This allows an expression for the current to be obtained in the s-space for the potential step applied using the relation,

$$I(s) = \frac{V(s)}{Z(s)} = \frac{-\Delta V(R_p C_d s\sqrt{s} + \sqrt{2}\sigma C_d s + \sqrt{s})}{R_p\sqrt{s} + \sqrt{2}\sigma + R_s(R_p C_d s\sqrt{s} + \sqrt{2}\sigma C_d s + \sqrt{s})} \quad (9)$$

An inverse Laplace transform of eq 9 would lead to a current expression in the time domain. However, eq 9 is too complex for one to convert to that in the t-space by a simple inverse Laplace operation.[16c] To be able to mathematically handle this situation, we define the following relations by introducing three new parameters, R_w, R_{cp}, and C_{cp}:

$$R_s = \frac{R_w R_{cp}}{R_w + R_{cp}}$$

$$R_p = R_w - \frac{R_w R_{cp}}{R_w + R_{cp}}$$

$$C_d = C_{cp}\left(1 + \frac{R_{cp}}{R_w}\right)^2 \quad (10)$$

We can show straightforwardly by using relations defined by eqs 10 that the equivalent circuits displayed in Figure 2a and b are identical. For the parallel circuit shown in Figure 2b, we have an expression for the total impedance of

$$\frac{1}{Z(s)} = \frac{1}{R_w + \sigma\sqrt{\frac{2}{s}}} + \frac{1}{R_{cp} + \frac{1}{C_{cp}s}} \quad (11)$$

(16) See: (a) Chapter 3, (b) Chapter 5, (c) Appendix A, and (d) Chapter 13 of ref 1.

(17) Delahay, P. *J. Am. Chem. Soc.* **1953**, *75*, 1430.

Thus, the current expression in the *s*-space should be

$$I(s) = \frac{V(s)}{Z(s)} = \frac{-\Delta V}{R_w s + \sigma\sqrt{2s}} + \frac{-\Delta V}{R_{cp} s + C_{cp}^{-1}} \qquad (12)$$

for a potential step ΔV. If the current before the step is $i(t \le 0)$, we obtain an expression for the current in the *t*-space,

$$i(t) - i(t < 0) = L^{-1}[I(s)] = \frac{-\Delta V}{R_w} \exp\left[\left(\frac{\sqrt{2}\sigma}{R_w}\right)^2 t\right] \operatorname{erfc}\left[\frac{\sqrt{2}\sigma}{R_w}\cdot\sqrt{t}\right] + \frac{-\Delta V}{R_{cp}} e^{-(1/R_{cp}C_{cp})\cdot t} \qquad (13)$$

upon inverse Laplace transform of eq 12.[16c] By restoring the original components from definitions given in eq 10, we have the final current expression,

$$i(t) - i(t \le 0) = \frac{-\Delta V}{R_p + R_s} \exp\left[\left(\frac{\sqrt{2}\sigma}{R_p + R_s}\right)^2 t\right] \operatorname{erfc}\left[\frac{\sqrt{2}\sigma}{R_p + R_s}\cdot\sqrt{t}\right] + \frac{-\Delta V R_p}{R_s(R_p + R_s)} e^{-(R_p+R_s)/(R_p R_s C_d)\cdot t} \qquad (14)$$

for the equivalent circuit shown in Figure 2a.

Now we also see in eq 14 both the faradaic and nonfaradaic components. It is interesting to note in eq 14 that both the solution (R_s) and polarization (R_p) resistances affect the capacitive current decay contrary to the generally accepted expression, $e^{-t/R_s C_d}$, in which only R_s and C_d determine the decay kinetics[14,16d] (see below for more on this). Further, the two resistors, R_s and R_p, act like they are connected in parallel in eq 14 although they are connected in series in the circuits shown in Figures 1 and 2a; the same is true for eq 4, which was not discussed as such at the time when the equation was first derived.[12a] The faradaic current, which appears very similar to eq 2, has two components, mass transport-independent and -dependent terms. By comparing the faradaic component of the current in eq 14 with that in eq 2, we recognize the following relations:

$$nFA(C_{ox}^{*} k_f - C_{red}^{*} k_b) = \frac{-\Delta V}{R_p + R_s} \qquad (15)$$

and

$$\exp(H^2 t)\ \operatorname{erfc}(H\sqrt{t}) = \exp\left[\left(\frac{\sqrt{2}\sigma}{R_p + R_s}\right)^2 t\right] \operatorname{erfc}\left[\frac{\sqrt{2}\sigma}{R_p + R_s}\cdot\sqrt{t}\right] \qquad (16)$$

Equation 16 leads to the relation,

$$H = \frac{k_f}{\sqrt{D_{ox}}} + \frac{k_b}{\sqrt{D_{red}}} = \frac{\sqrt{2}\sigma}{R_p + R_s} \qquad (17)$$

Figure 3a shows faradaic and nonfaradaic components as well as the total current calculated using eq 14 for the circuit shown in Figure 2a with $\Delta V = 5.0$ mV, $R_s = R_p = 10.0\ \Omega$,, and $C_d = 20\ \mu$F. The nonfaradaic current calculated from eq 14 is also compared with that calculated without the contribution from R_p in Figure 3b. It is seen from this comparison that the capacitive currents could be significantly different depending on whether the contribution of R_p is taken into account or not and also depending on how large or small the R_p value is in comparison with R_s. Before the electron-transfer reaction begins to take place, R_p is much larger than R_s and the *RC* time constant is determined by only R_s, but both R_s and R_p values become important when the potential reaches a value at which R_p begins to compete with R_s. At a very large overpotential, the contribution from R_p dominates the *RC* time constant. A graph displaying the relative contributions of the R_p and R_s to the capacitive decay time is shown in Figure 4.

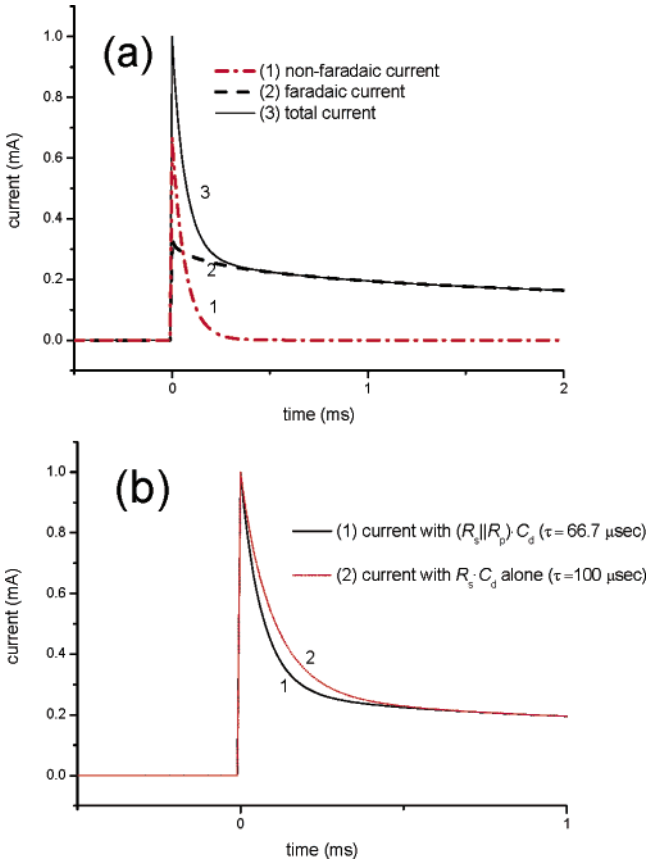

Figure 3. (a) Nonfaradaic (1) and faradaic (2) components calculated upon application of a 5.0-mV potential step using eq 14 with $R_s = R_p = 10.0\ \Omega$ and $C_{dl} = 20\ \mu$F, and their sum (3) and (b) comparison of nonfaradaic currents when the time constants with (1) and without (2) consideration of R_p (i.e., $\tau = R_s C_d$ and $R_s||R_p C_d$) were used.

The faradaic component calculated using eq 14 is also compared with that calculated from eq 2 (Figure 5). These curves were constructed from arbitrarily assigned kinetic values, i.e., $R_s = R_p = 10\ \Omega$, $C_d = 20\ \mu$F, $D_O = D_R = 1.0 \times 10^{-6}$ cm^2/s, and A (electrode area) $= 0.020$ cm^2. These values yield a k^0 value of 8.83×10^{-3} cm/s and k_f and k_b values of 9.74×10^{-3} and 8.02×10^{-3} cm/s, respectively, for an overpotential (ΔE) of 5.0 mV. The rate constants thus obtained and the diffusion coefficients yield an H value of 17.8 s$^{-1/2}$. It is seen from Figure 5 that the two plots generated using two current expressions using these kinetic parameters are identical. These comparisons confirm that (1) eq

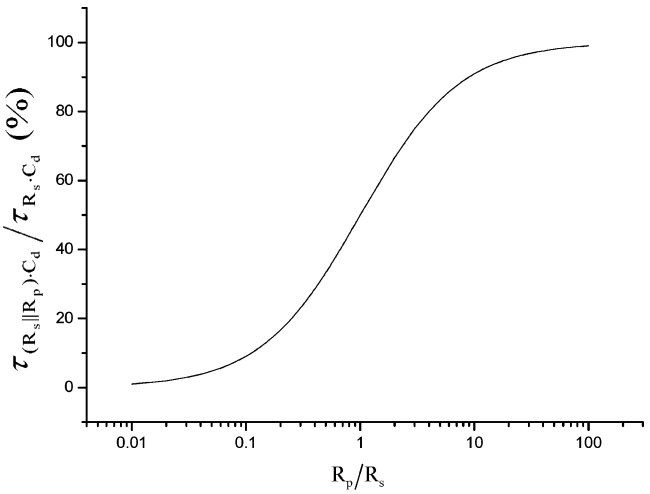

Figure 4. Ratio of the *RC* time constants plotted for the ratio of *R* values obtained from the parallel connection of R_p and R_s ($\tau_{(R_s||R_p)}C_d$) to that calculated with only R_s considered ($\tau_{R_s\cdot C_d}$).

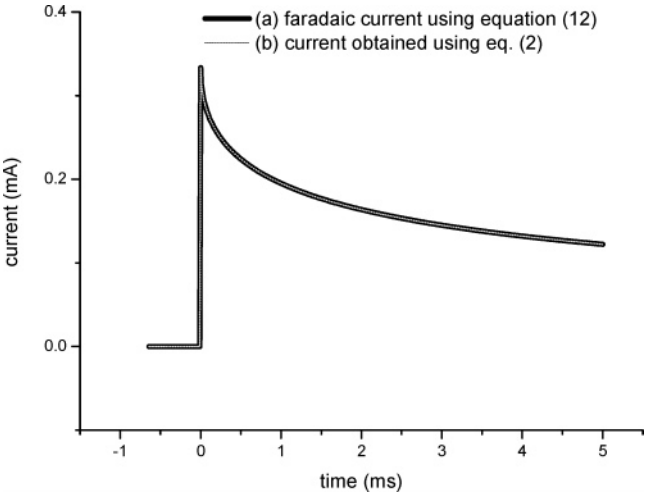

Figure 5. Faradaic currents obtained upon application of a 5-mV step for an electrochemical system calculated from eqs 2 and 14. (a) The current obtained from the equivalent circuit shown in Figure 2a using eq 14 (solid) and (b) that calculated from eq 2 (dotted line). The kinetic parameters used for these calculations were the same as those used for Figure 3.

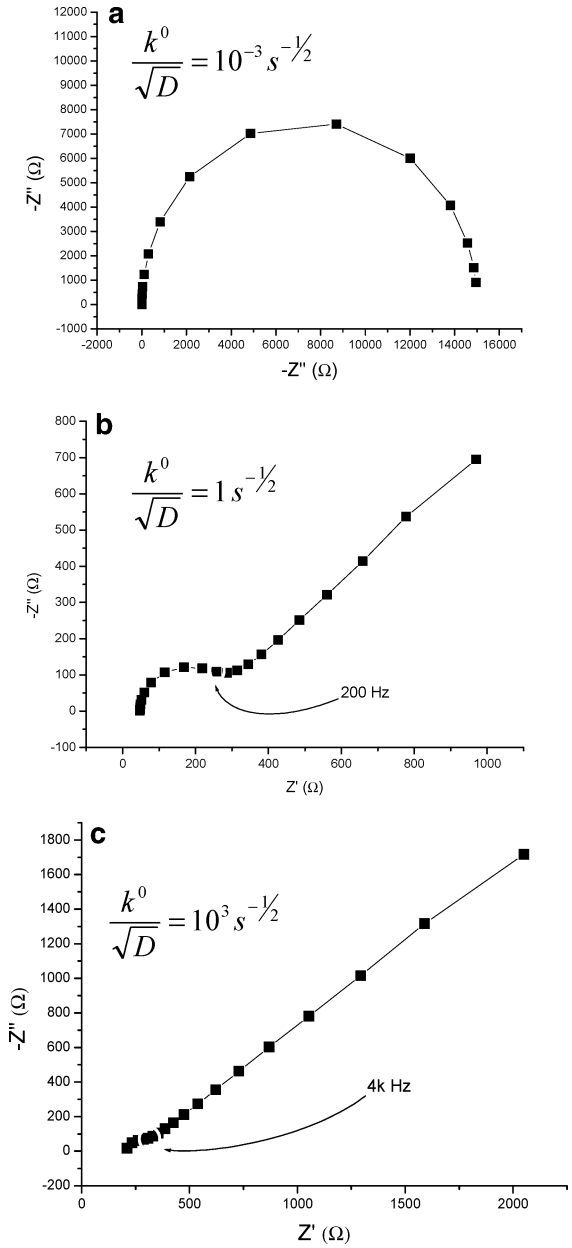

Figure 6. Nyquist plots calculated from currents generated from eq 14 with the kinetic parameters ($k^0/D^{1/2}$) shown in the figure. The calculations were performed between 50 kHz and 1 Hz.

14 is identical to eq 2 for a small potential step for an electron-transfer reaction when the nonfaradaic component is excluded from the current expression and (2) the nonfaradaic current calculated from the double layer capacitance and the solution resistance alone does not correctly reflect physical pictures of actual electrochemical cells.

Another way of confirming the validity of eq 14 is to numerically generate the impedance data[14] for electrochemical reactions, in which electron-transfer rate constants are varied and compare how they behave in each case. This is because the mass transport effect (Warburg impedance) would start to show up at different frequencies depending on the R_p value in eq 14. The Nyquist plots obtained using the currents generated from eq 14 for different electrokinetic values in comparison to diffusion coefficients are shown in Figure 6. This figure clearly shows that all the components including the Warburg impedance *do* show up in the Nyquist impedance plots starting at different frequencies depending on how the electron-transfer rate constant compares with the diffusion coefficient of the electrochemical system. As can be seen, the sampling period should be extended significantly for the Warburg contribution to become visible for a slow electron-transfer reaction (Figure 6a).

To see how the sampling periods would affect the impedance results in the small potential step impedance measurement experiments, we present the impedance plots in Figure 7a, calculated using the current data generated from eq 14 with the same kinetic data as those used for the calculation of the currents shown in Figures 3 and 5. For the current sampled to 1.0 ms (the lowest frequency of 1 kHz, ○), we see only a high frequency part of the data, which follows exactly the same semicircle as that calculated from the current data sampled to 100 ms (Figure 7a, ■). Thus, the impedance plot calculated for a short sampling period follows that obtained from the currents sampled to a longer period except that no Warburg component is seen in the lower

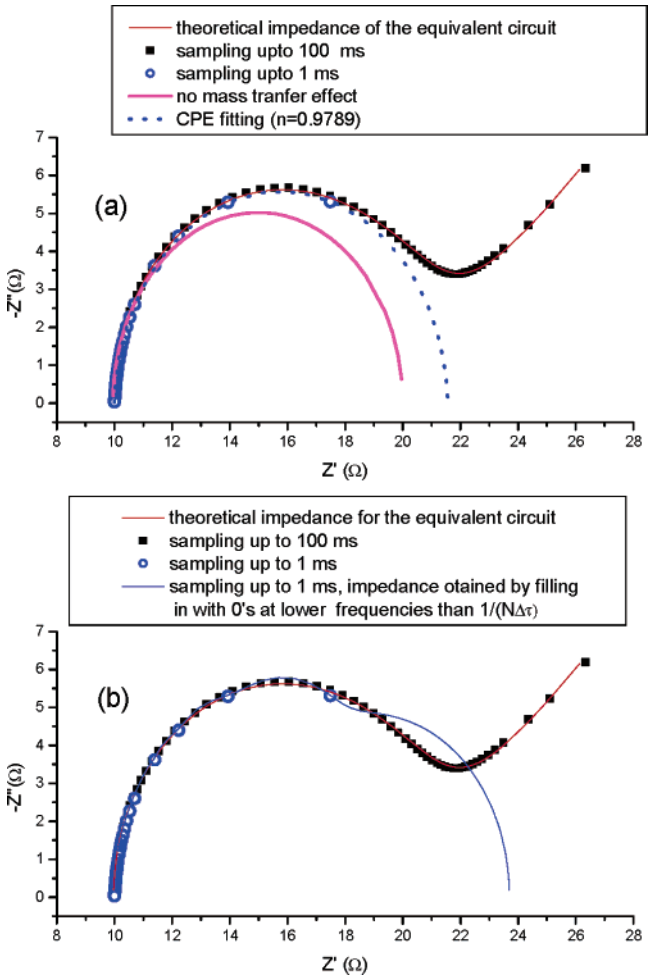

Figure 7. Nyquist plots calculated from the currents generated from eq 14. (a) Data acquired for up to a sampling time of 100 ms (■) and to 1.0 ms (○) and without mass transport effects (—); and (b) the plot calculated for up to the sampling time of 100 ms as shown in (a) (■) and that obtained (—) when the derivative data were filled up with 0's beyond the sampling time of 1.0 ms and then the DTFT was performed. Note the second semicircle starting from 1 kHz (= 1.0 ms) where the sampling of the signal was terminated.

frequency region. On the other hand, the impedance line shown by the smallest semicircle (solid line) is obtained when the impedances are calculated without the mass transport effects considered (Figure 1) using the same electrokinetic data.

A few interesting observations can be made from the plots shown in Figure 7a. First, the mass transport affects the impedance (semicircle) from the very high frequencies, as can be seen by the lines represented by sampling periods of 1.0 and 100 ms, which start to deviate from the impedance without mass transport effects (solid line). Thus, the impedance plots that do not appear to have a Warburg component are not necessarily without mass transport effects; the Warburg components are simply not seen within the frequency range covered by the inverse of the sampling period due to the sluggish electron-transfer kinetics. We believe that many impedance plots reported in the literature share this problem. In fact, we found that the line obtained for the 1.0-ms sampling period can be fitted perfectly only when a Warburg impedance was taken into account even though it is physically not seen simply because the data were not acquired at lower frequencies than 1 kHz. Without factoring in the Warburg component, the semicircle was somewhat depressed and simulated well only if the capacitance was replaced by a constant phase element[18] (CPE) with an n value of 0.979. The CPE with $n = 0.979$ implies that the interface has some pores, which impede the ion transport to some extent. With the CPE factored in, an R_p value of 11.6 Ω, which is 16% greater than the true value, is obtained. However, we obtain correct R_s, R_p, and C_d values when a Warburg impedance of 0.01 $S \cdot s^{1/2}/cm^2$ is used in the calculation even though they are not seen in the impedance plot. This indicates that many CPEs reported in the literature might also have resulted from the mass transport effects, which is simply not seen within the frequency region studied.

Another point is the effect of how the data are extrapolated, when the discrete time Fourier transform (DTFT) calculation is performed as demonstrated in Figure 7b. The DTFT operation can introduce an additional semicircle into the lower frequency region than 1.0 kHz as shown in Figure 7b, which is an artifact introduced by the calculation as pointed out by Jurczakowski and Lasia,[14] when one assumes certain values from a priori knowledge as to how the chronoamperometric current would behave beyond the sampling period. This observation shows that only the data obtained from the experiments should be used for the FT calculations. This also suggests that the derivative signals do not decay to 0 even though they look like 0 beyond a certain period, which leads to a hardware requirement that the bit resolution of the analog-to-digital converter should be high enough to read small changes in current for longer sampling periods.

Experimental Verification. To evaluate the theory we developed, we made a few rudimentary measurements on three electrochemical systems having electroactive species with different electron-transfer rate constants. We chose three redox reactions, i.e., reduction of $Ru(NH_3)_6^{3+}$ and *p*-BQ at gold electrodes, and oxidation of Fe^{2+} at BDD electrodes, which were shown to have heterogeneous electron-transfer rate constants of >1 cm/s,[19] 9.7×10^{-4} cm/s,[20] and 2.3×10^{-5} cm/s (see below), respectively, which roughly satisfy the rate requirements of $k^0/D^{1/2}$ of $>10^3$, ~ 1, and $<10^{-3}$ $s^{-1/2}$, meeting the approximate conditions set for Figure 6. The experimental conditions used for the determination of the rate constant for the *p*-BQ were almost identical to the ones used in this work.[20] *p*-BQ has been shown to undergo a one-electron transfer to produce an anion radical in neutral aqueous media.[20,21] Figure 8 shows cyclic voltammograms (CVs) for these redox pairs. As can be seen, the reduction reactions of *p*-BQ and $Ru(NH_3)_3^{3+}$ are both electrochemically and chemically reversible on the experimental time scale used to record voltammograms in Figure 8, while the oxidation of Fe^{2+} at the BDD electrode is chemically reversible but electrochemically irreversible with a

(18) The CPE arises because the double layer formed at an electrode/electrolyte interface does not behave as an ideal capacitor when it contains a large number of surface defects or pores comparable to the sizes of the ions. When the CPE is expressed in terms of the admittance, Y_{CPE}, it has an expression, $Y_{CPE} = Y_C\omega^n \cos(n\pi/2) + jY_C\omega^n \sin(n\pi/2)$. Depending on the value of n, the CPE can have a variety of responses. With $n = 0$, it represents a resistance with $R = Y_C{}^{1-}$; with $n = 1$, a capacitance with $C = Y_C$ while a Warburg resistance with $n = 0.5$. See ref 3 for details.

(19) Chailapakul, O.; Crooks, R. M. *Langmuir* **1995**, *11*, 1329.
(20) Krysiński, P.; Rrzostowska-Smolska, M. *J. Electroanal. Chem.* **1997**, *424*, 61.
(21) (a) Pyun, C.-H.; Park, S.-M. *J. Electrochem. Soc.* **1985**, *132*, 2426. (b) Shim, Y.-B.; Park, S.-M. *J. Electroanal. Chem.* **1997**, *425*, 201. (c) Kim, Y.-O.; Jung, Y. M.; Kim, S. B.; Park, S.-M. *Anal. Chem.* **2004**, *76*, 5236.

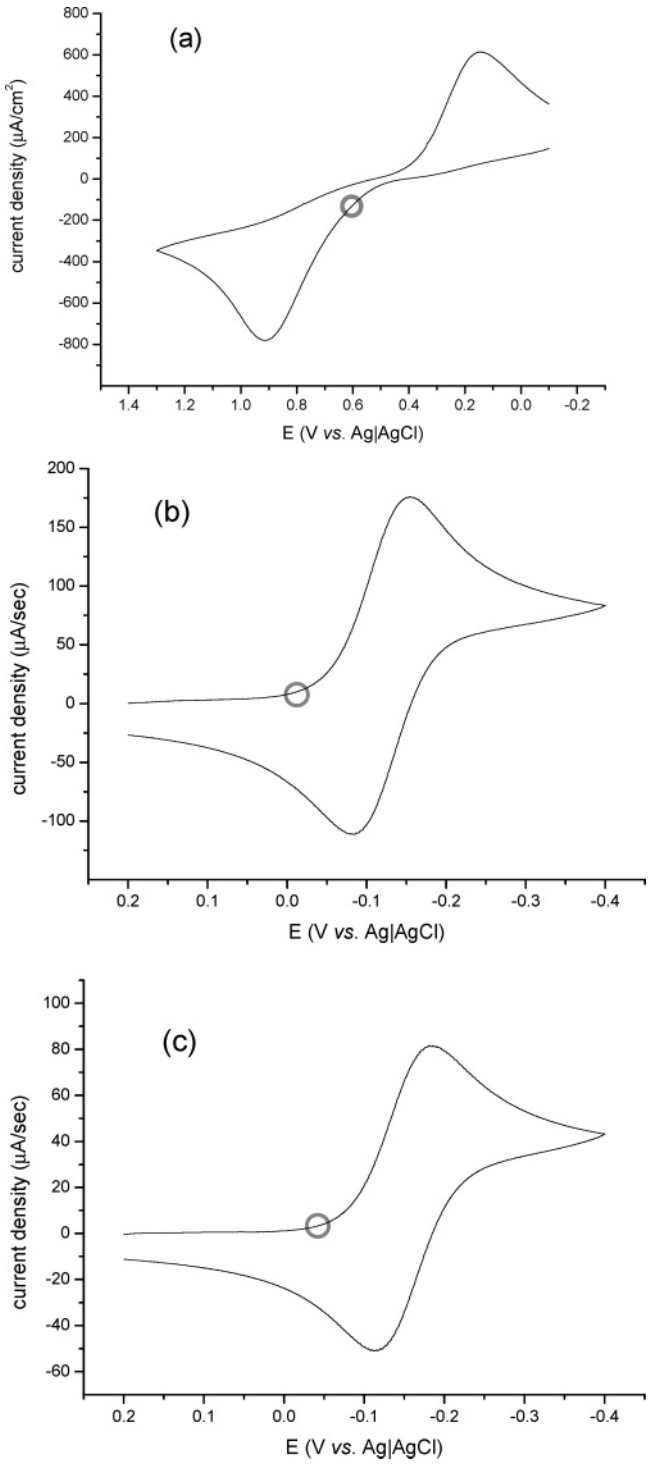

Figure 8. Cyclic voltammograms recorded in solutions containing (a) 5.0 mM Fe^{2+} and 0.50 M H_2SO_4, (b) 5.0 mM *p*-BQ and 0.50 M KCl, and (c) 5.0 mM $Ru(NH_3)_3^{2+}$ and 0.50 M KCl. A BDD electrode (area 0.12 cm^2) was used for Fe^{2+} oxidation whereas a gold electrode (area 0.025 cm^2) was used for the other two experiments. The impedance plots shown in Figure 9 have been measured at the potentials indicated by a circle. The scan rate was 75 mV/s.

large peak separation, which is in good agreement with those recorded under similar experimental conditions.[22] The exchange rate constant for the Fe^{2+} oxidation has been determined to be 2.3×10^{-5} cm/s with α (transfer coefficient) = 0.60 by digital simulation of the forward CV current shown in Figure 8a using a

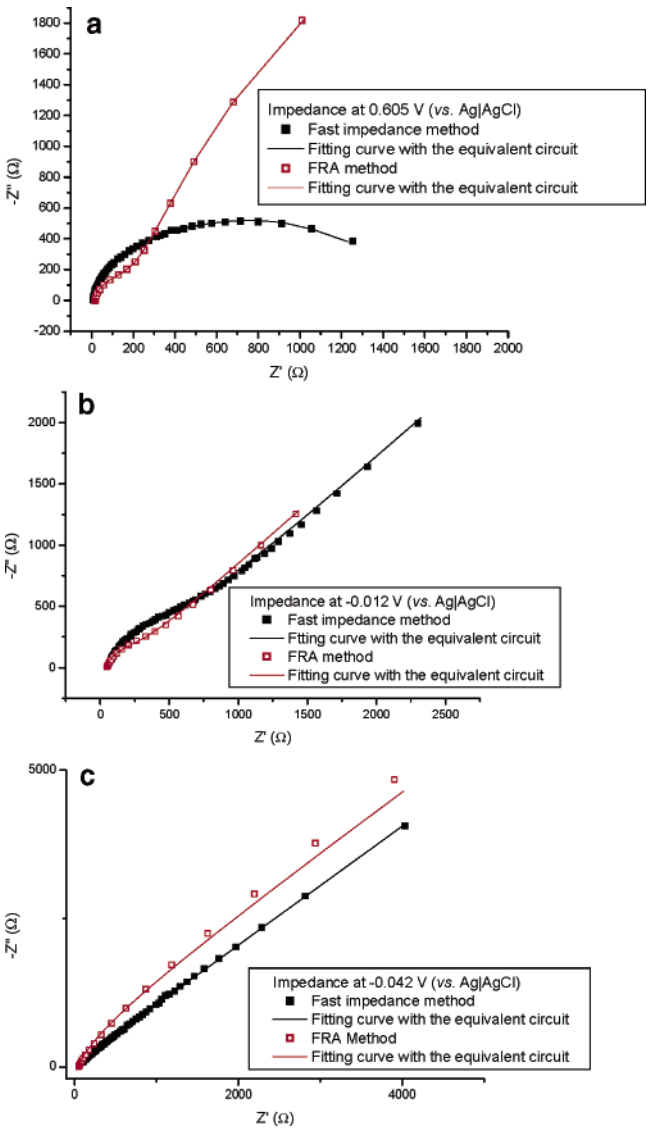

Figure 9. Actual impedance data obtained between the frequency range of 5 Hz < *f* < 10 kHz for (a) oxidation of Fe^{2+} at 0.605 V, (b) reduction of *p*-BQ^0 at −0.012 V, and (c) 5.0 mM $Ru(NH_3)_6^{3+}$ at −0.042 V vs Ag|AgCl by fast impedance (■) or FRA (□) methods. See Figure 8 for experimental conditions.

Digisim simulation program when $D_R = 5.6 \times 10^{-6}$ cm^2/s was used.

The impedance measurements shown in Figure 9 have been carried out at the points indicated by circles on the CVs shown in Figure 8 to avoid too high electron-transfer rates, which would cause the impedance plots dominated by the Warburg impedances, particularly when measured by the FRA method as had been shown previously.[12a] The results were obtained within the frequency range of

$$\frac{1}{N \cdot \Delta t} \leq f \leq \frac{1}{2\Delta t} \tag{18}$$

which defines the effective range of the sampling period not to violate the Nyquist sampling theorem. Thus, we took the signal

(22) Lee, J.; Tryk, D. A.; Fujishima, A.; Park, S.-M. *Chem. Commun.* **2002**, 486.

between 0 and 200 ms to obtain the data between 5.0 Hz and 10 kHz with a Δt value of 1.0×10^{-4} s. The results of these measurements are shown in Figure 9 along with those obtained by the FRA method. The χ^2 values obtained for the impedance data to see how well the observed data fit to the theoretically expected ones are 8.4×10^{-4}, 6.7×10^{-4}, and 2.8×10^{-4}, respectively, for Fe^{2+} oxidation, *p*-BQ reduction, and Ru^{3+} reduction, when the data are obtained by the fast impedance measurements, whereas they are 5.4×10^{-4}, 1.8×10^{-3}, and 3.8×10^{-3} for the data obtained from the FRA method. This indicates that the data obtained from the fast impedance measurements should be as reliable as those from the FRA method if not better. It is seen in general that the impedances obtained by the FRA method display smaller R_p values as seen from the smaller radii for the corresponding semicircles. Also, the Warburg impedances show up at relatively higher frequencies in the results obtained by the FRA method. We believe this is due to the fact that the FRA machines wait until a steady-state current is obtained from the system or the mass transport reaches a steady state. As a result, the impedance data are obtained from what is termed a *stationary* system[5] after the system has reached a mass transport limited current. This causes smaller impedances to be obtained for the electron transfer with the Warburg components showing up in the plot. On the other hand, the fast impedance methods provide information on the impedances of the transient or *nonstationary* system by taking snapshots at the instant when the potential step is applied. One obvious point on measurements made on stationary systems is that the data would represent the time-averaged results for the whole measurement period and the responses obtained at high frequencies may not always be the same as those at low frequencies as a true stationary system may never be obtained during an electrochemical reaction.

It is seen from the results of these measurements that the Warburg impedance is not seen during Fe^{2+} oxidation (Figure 9a), which undergoes a slow electron-transfer reaction. On the other hand, the Warburg impedances are observed at relatively high frequencies well before the sampling is completed for both cases of *p*-BQ and $Ru(NH_3)_6^{3+}$ reduction (Figure 9b and c), where the electron-transfer rate constants are reasonably fast, i.e., greater than 1×10^{-3} cm/s.

A closer examination of the Nyquist plot shown for Fe^{2+} oxidation (Figure 9a) reveals that it is significantly depressed, suggesting that the semicircle must result from more than one electron-transfer processes. The other possibilities could be that either the capacitors in the circuit actually act like CPEs as we have seen earlier or the mass transport affects its shape as we discussed above for the current data generated using eq 14 (Figure 7a). In efforts to clarify this, we fitted the experimental data with three different equivalent circuits shown in Figure 10a–c and the results are shown in Figure 10d. The best fit was obtained when the equivalent circuit shown in Figure 9c was used with R_s, R_{p1} R_{p2}, and R_{p3} values of 9.1, 37.8, 567, and 516 Ω, and C_{d1}, C_{d2}, and C_{d3} of 106, 134, and 34 μF, as well as W of 0.0060 $S \cdot s^{1/2}/cm^2$, respectively. In other words, the Fe^{2+} oxidation should actually be made of a three-step electron-transfer process with three different rise times ($\tau = R_{pi}C_{di}$). The fact that the three processes are coupled in Fe^{2+} reduction suggests that the electron transfer

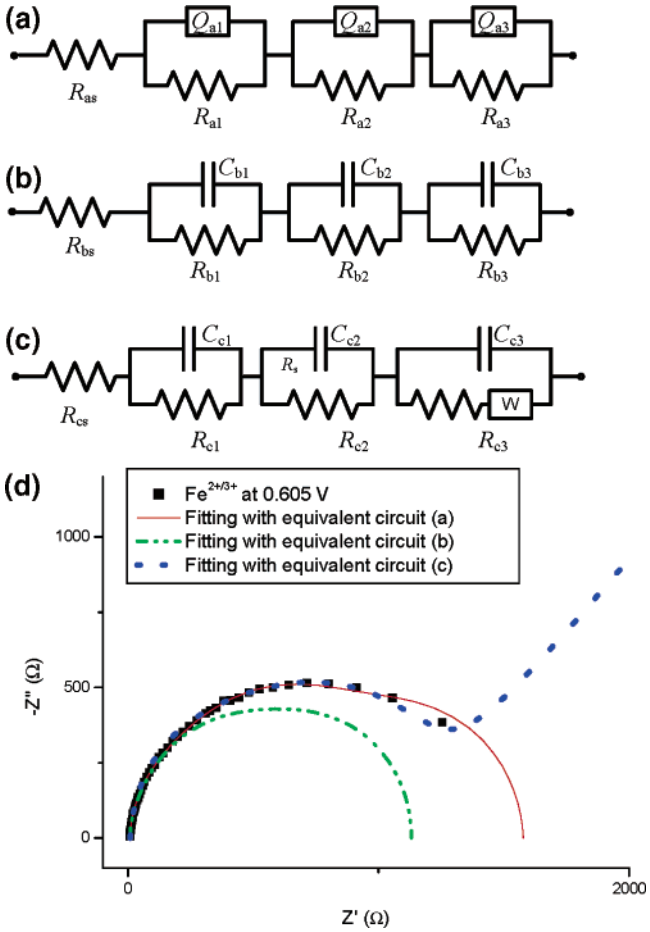

Figure 10. (a–c) Proposed equivalent circuits to fit the impedance plot shown in Figure 9a and (d) the results of data fitting using the above three equivalent circuits shown in (a) (—), (b) (—··—··), and (c) (- - -). Here the element Qs are CPEs (see the text).

takes place via more than one intermediate species due perhaps to their continuous changing solvation structures, which present the activation energies in each step, consistent with the Marcus theory.[23] This explains why electron-transfer reactions such as proton reduction at a mercury electrode or water oxidation at many metal electrodes can be sluggish; they must undergo the reaction via a series of intermediate species. The overall polarization resistance (R_p) would thus be the sum of these three, i.e., 1130 Ω. Employing eq 17, we calculate k_f values by obtaining σ and R_p values from the impedance data in a wide range of bias potentials, which allow the calculation of a number of k^0 values, leading to an average k^0 value of 5.6 ($\pm$1.0) $\times 10^{-5}$ cm/s with the same α and D_R values as those used for digital simulation. The rate constant thus obtained is in reasonably good agreement with that obtained from the digital simulation considering that the methods used are completely different from each other. The kinetic parameters, k^0 and α, would be more accurately determined when the measurement is made in solutions containing different total concentrations of equimolar amounts of the reductant and the oxidant at the equilibrium potential. This set of experiments should remove assumptions made above and also allow the α values to be determined.[14a]

(23) (a) Marcus, R. A. *J. Chem. Phys.* **1965**, *43*, 679. (b) Marcus, R. A. *Annu. Rev. Phys. Chem.* **1964**, *15*, 155.

CONCLUSIONS

We have demonstrated in this work that an integrated current expression containing both the faradaic and nonfaradaic components for a potential step experiment can be derived based solely on the equivalent circuit, which was originally designed to explain an electrochemical reaction. The results showed from a variety of calculations that the current expression we obtained correctly represents both the faradaic and nonfaradaic currents for an electron-transfer reaction at an electrified interface. This indicates that an electrochemical system can indeed be modeled correctly by an equivalent circuit theory. The faradaic current expression obtained from the equivalent circuit is shown to be the same as that obtained from diffusion equations, which have been used for a long time. The *RC* time constant for the nonfaradaic current decay, however, is shown to be determined by a resistor obtained from the parallel connection of the solution and polarization resistors, along with the double layer capacitance, which is not in agreement with our traditional understanding that it must be a simple product of the solution resistance and the double layer capacitance. It was also shown that the mass transport affects the current, thus the impedance, from the very beginning of the potential step, resulting in what appears to make the semicircle depressed. The semicircle that does not display a Warburg impedance is also shown to perfectly fit the experimental data only with the mass transport effect (Warburg impedance) taken into account even though the Warburg component is not seen in the Nyquist plot because the sampling is completed before the Warburg impedance gets into the picture.

Our results here have a few implications. First, the equivalent circuits do indeed represent correct models for electron-transfer reactions. They were first borne out to explain the impedances measured for electron-transfer results.[15] The fact that the faradaic current originating from this theory is identical to that obtained from the diffusion equations proves that equivalent circuits do indeed represent the electron-transfer reactions correctly. Second, nonfaradaic or capacitive currents are determined by both the solution and polarization resistances unless no faradaic process is involved. Thus, the polarization resistance plays an important role in determining the capacitive current once the faradaic process has begun to take place. In this sense, we may need to reevaluate the contributions of capacitive currents and their corrections made in the literature. Third, our results demonstrate that the Warburg impedance should be taken into account when the impedance data are being theoretically analyzed unless the mass transport is clearly excluded from the process of interest on a known basis. The results we obtained here are expected to have important impacts on the description of electrode/electrolyte interfaces and the interpretation of the currents and subsequent corrections of faradaic currents in electroanalytical chemistry.

ACKNOWLEDGMENT

This work was supported by the SRC/ERC program of MOST/KOSEF (Grant R11-2000-070-06001-0) and the stipends for the graduate assistants were supplied by the BK21 program of the Korea Research Foundation. We are also indebted to Dr. Jung-Suk Yoo for useful discussions during this work.

Received for review September 14, 2005. Accepted November 11, 2005.

AC051641L